Published for the International Glaciological Society

Tidal flexure reveals effective elasticity in grounding zones on the Ross Ice Shelf

Journal:	*Journal of Glaciology*
Manuscript ID	JOG-2025-0046
Manuscript Type:	Article
Date Submitted by the Author:	11-Apr-2025
Complete List of Authors:	Elgart, Faye; Massachusetts Institute of Technology, Earth, Atmospheric, and Planetary Sciences Minchew, Brent; Massachusetts Institute of Technology, Department of Earth, Atmospheric and Planetary Sciences Meyer, Colin; Dartmouth College, Thayer School of Engineering
Keywords:	Ice shelves, Antarctic glaciology, Laser altimetry
Abstract:	The grounding zones of Antarctic ice shelves are among the continent's most dynamic regions, where floating ice shelves buttress grounded upstream ice and tidal forcing drives cyclic flexure at the ice-ocean-bed interface. We use ICESat-2 altimetry and airborne ice-penetrating radar to constrain the effective Young's modulus E* of ice in the flexure zone at three sites on the Ross Ice Shelf. By modeling ice as an elastic beam of variable thickness, we infer a single effective elastic parameter, E*, that encapsulates the combined flexural response of the ice-bed-ocean system. Our results show considerable spatial variability in E*, with values ranging from ~1–9 GPa across sites, and an average of 3.6 ± 2.5 GPa. This variability reflects intersecting basal, oceanographic, and mechanical processes in the grounding zone, including bed stiffness, subglacial hydrology, and viscoelasticity of ice. Because flexure of bed and ice cannot readily be distinguished in observations, we argue for a bulk interpretation of E* that allows uncertainty to be quantified in terms of a single parameter. These results offer a new method for estimating ice shelf thickness and thickness gradient near the grounding line,

	independent of the hydrostatic assumption, with implications for basal melt rate estimates and future sea-level rise projections.

Journal of Glaciology, Vol. 1, No. 1, 2025

Tidal flexure reveals effective elasticity in grounding zones on the Ross Ice Shelf

Faye M. ELGART,[1] Brent M. MINCHEW,[1] Colin R. MEYER[2]

[1] *Department of Earth, Atmospheric, and Planetary Sciences, Massachusetts Institute of Technology, Cambridge, MA, USA*

[2] *Thayer School of Engineering, Dartmouth College, Hanover, NH, USA*

Correspondence: Faye M. Elgart <fmhe@mit.edu>

ABSTRACT.

The grounding zones of Antarctic ice shelves are among the continent's most dynamic regions, where floating ice shelves buttress grounded upstream ice and tidal forcing drives cyclic flexure at the ice-ocean-bed interface. We use ICESat-2 altimetry and airborne ice-penetrating radar to constrain the effective Young's modulus E* of ice in the flexure zone at three sites on the Ross Ice Shelf. By modeling ice as an elastic beam of variable thickness, we infer a single effective elastic parameter, E*, that encapsulates the combined flexural response of the ice-bed-ocean system. Our results show considerable spatial variability in E*, with values ranging from 1–9 GPa across sites, and an average of 3.6 ± 2.5 GPa. This variability reflects intersecting basal, oceanographic, and mechanical processes in the grounding zone, including bed stiffness, subglacial hydrology, and viscoelasticity of ice. Because flexure of bed and ice cannot readily be distinguished in observations, we argue for a bulk interpretation of E* that allows uncertainty to be quantified in terms of a single parameter. These results offer a new method for estimating ice shelf thickness and thickness gradient near the grounding line, independent of the hydrostatic assumption, with implications for basal melt rate estimates and future sea-level rise projections.

INTRODUCTION

Grounding zones are transition regions where grounded ice sheets become floating ice shelves and ice, ocean, and the solid Earth all meet. The dynamics of the grounding zone are among the most sensitive indicators of change in the Antarctic (Pattyn, 2017; Scambos and others, 2017; Gudmundsson and others, 2019; Seroussi and others, 2020). The satellite era has revealed widespread, rapid grounding line retreat (Joughin and others, 2014; Rignot and others, 2014), especially in West Antarctica, where ice shelves are increasingly melted from below by warm, salty Circumpolar Deep Water (Nakayama and others, 2018; Jourdain and others, 2017). Basal melt rate in the grounding zone is one of the largest sources of uncertainty in future projections of the rate and amount of future sea-level rise (Pritchard and others, 2012; Adusumilli and others, 2020; Seroussi and others, 2020; Hill and others, 2021).

Basal melt rate m can be calculated by conservation of mass provided that the local ice thickness h is well-known such that:

$$\frac{\partial h}{\partial t} = (a - m) - \nabla \cdot (h\underline{u}) \tag{1}$$

where a is the surface mass balance, and u is the ice velocity. Ice shelf thickness is typically calculated by a freeboard approach, where the ice height above the ocean surface is measured and the total ice thickness is calculated as the freeboard height times $\rho_{sea}/(\rho_{sea} - \rho_{ice})$, with a correction for firn densification (Smith and others, 2020; Chartrand and Howat, 2023). This works well near the calving front, where ice is in hydrostatic equilibrium and floats up and down on ocean tides. However, near the grounding line, the ice shelf is mechanically coupled to the upstream ice sheet and flexes, rather than floats (figure 1).

The flexure of an elastic beam under a load depends on its flexural rigidity, proportional to the product of its thickness cubed and Young's modulus E. In 1995, David Vaughan modeled the tidal flexure of ice with an elastic beam of constant thickness and rode a snowmobile back over its own tracks at different points in the tidal cycle on the Rutford Ice Stream while measuring the vertical position of the ice surface and found that a value for E of 0.88 ± 0.35 GPa adequately minimized the misfit between modeled and observed flexure using a constant ice thickness h from contemporaneous radar sounding measurements, as only one of h or E can be inferred from this inversion given the other (Vaughan, 1995).

This result is somewhat surprising, as the value of the Young's modulus of ice is commonly taken to be 9 GPa: an order of magnitude greater (Cuffey and Paterson, 2010). The Young's modulus of a material is an elastic parameter that reflects the ratio of an applied uniaxial normal stress to instantaneous normal strain, and has its physical basis in the electromagnetic forces between molecules in its crystal lattice. It is measured in the laboratory by mechanical stress-strain curve testing, or by wave speed measurement through the lattice, or by interferometric phonon scattering measurements (Schulson and Duval, 2011; Rathmann and others, 2022; Gammon and others, 1983). As ice is a viscoelastic material, there is a dependence of E on the rate of the applied stress due to creep and anelastic effects happening over time, as well as on temperature and presence of water or inclusions (Sinha, 1989, 1978). Sinha (1978) uses the term *effective* Young's modulus to distinguish between the "true" instantaneous elastic modulus at high frequencies and the relationship between stress and strain of in situ ice. Gold (1977) compiles a number of laboratory experiments and finds an approximately linear relationship between Young's modulus and the frequency of applied stress leading to $E \approx 3$ GPa at 10^{-3} Hz. The tidal frequency is about 10^{-5} Hz, which would give $E \approx 1$ GPa if the linear relationship continues, as noted by Vaughan (1995).

Numerous approaches have been employed to resolve the apparent discrepancy between the laboratory values of $E = 9$ GPa and the much smaller results from tidal flexure models. Reeh and others (2003) develops a linear viscoelastic model similar to a Burgers model with four elastic parameters and uses flexure data on Nioghalvfjerdsfjorden glacier from tiltmeters and GPS, with airborne ice-penetrating radar thickness, and temperature measurements from a borehole to determine the local ice viscosity. Detailed information on the phase of the viscous adjustment to the tide is also needed, which is possible with tiltmeters but not with satellite laser altimetry. The launch of ICESat in 2005, followed by ICESat-2 in 2018, made it possible to difference repeat track measurements of ice surface height at different points in the tidal cycle to observe tidal flexure near the grounding line on many ice shelves around Antarctica (Fricker and Padman, 2006). Sayag and Worster (2013) modeled the flexure as an elastic beam of constant thickness and used ICESat altimetry in two places on the Ronne-Filchner Ice Shelf and found a best fitting value for E of 1.8 GPa in a "stiff-fixed" model, where the grounding line is fixed and ice rests on a stiff frozen bed, but a best fitting E of 9.33 GPa with a "soft-free" model, where the grounding line is allowed to move and ice rests on an elastic bed having an estimated spring constant of 1 MPa/m. Marsh and others (2014) used differential interferometric synthetic aperture radar (InSAR) to observe tidal flexure on Beardmore Glacier and allowed the ice thickness to vary and using a value for E of 1.4 GPa are able to invert for local ice thickness using COMSOL, a commercial multi-physics finite-element software package.

A number of studies have incorporated viscoelastic effects and compared these to elastic models. Wild and others (2018) compare a viscoelastic and an elastic model, with an elastic bed of spring constant 5 MPa/m, and find the viscoelastic model is very sensitive to the tidal model used to determine the phase of the tide. Rosier and others (2017) compare a simple elastic beam model to full-Stokes viscoelastic models with inclusion of basal crevasses and density dependent ice stiffness and find that the elastic solution model can produce similarly excellent fits to data, as well as that a factor of two of variation, ranging from about 2-4 GPa, in estimated effective Young's modulus exists even when local ice thickness is well constrained.

Here, we use satellite observations of the surface flexure of ice along with a simple physical model of ice in the flexure zone as an elastic beam of varying thickness, motivated by the need for better estimates of ice thickness and thickness gradient near the grounding line, to constrain the effective Young's modulus of ice in three places on the Ross Ice Shelf. We infer a single effective elastic parameter, the effective Young's modulus E*, to parameterize the observable flexure of the combined ice-bed-ocean system near the grounding line, and argue that we can not readily distinguish flexure of the ice from flexure of the bed. This allows much of the uncertainty inherent to the problem to be wrapped into one effective parameter whose associated uncertainty can be quantified. We use airborne ice-penetrating radar measurements of ice thickness $h(x)$ on the Ross Ice Shelf (RIS) (Das and others, 2020) to constrain the effective rheology of ice in the flexure zone by minimizing the misfit between modeled flexure and observed ice flexure with laser altimetry data from ICESat-2. We consider this work to be the first major step in a method towards an independent, observationally constrained estimate of ice thickness near the grounding line for basal melt rate, which can ultimately be linked to reducing uncertainty about the rate and amount of future sea level rise.

We show that a simple, observationally constrained model of the grounding zone as an elastic beam under tidal forcing reveals substantial variation in effective Young's modulus in three areas on the Ross Ice Shelf. The in situ environment of ice near the grounding line is complex and influenced by physical forces on intersecting length and timescales (Figure 1). Ocean tides cycle around Antarctica every 12-24 hours (Padman and others, 2018). Tides pump seawater in and out of the flexure zone, acting as a forcing to the hydrodynamics of a poroelastic bed with sediment on a spectrum from fully frozen to fully deformable (Warburton and others, 2020). There is tidal mixing of incoming and outgoing water masses: warm, salty Circumpolar Deep Water increasingly encroaches on the Antarctic continental shelf and melts ice from below, releasing cold glacial meltwater which can refreeze onto the ice shelf (Nakayama and others, 2018). There are surface and basal crevasses and channels that direct the flow of water (Alley and others, 2023).

The first direct underwater observations of the grounding zone have begun to show a complex system where these and other processes interact on different length and timescales to produce angular terraced forms on the undersides of ice shelves, as well as swooping, curved regions where convective and oceanographic forcings act differently on the flexure zone system (Wåhlin and others, 2024).

The observable surface flexure of ice near the grounding line reflects the combined effects of these competing processes, as well as any flexure of the sediment and bed. For this reason, as well as the viscous and anelastic processes that necessarily affect the stress-strain relationship in real time, we will refer only to an effective Young's modulus E*, to reflect the fact that the relationship between stress and strain that can be inferred from tidal flexure is a bulk parameter not identical to the Young's modulus of ice as can be measured in the lab, and may indeed vary considerably in space.

METHODS

We employ an elastic beam bending model constrained by repeat track flexure data from ICESat-2 to estimate the flexural rigidity of ice in the flexure zone of the Ross Ice Shelf. These locations are selected to be far from confining topography, perpendicular to the grounding line, and close to ice thickness measurements, in order to narrowly apply the linear elastic approximation. Using ice-penetrating radar thickness data from the ROSETTA-Ice airborne geophysical survey (Das and others, 2020), we then calculate the effective Young's modulus of ice in the flexure zone.

Model

We model ice in the flexure zone as an elastic beam of varying thickness, under small deformations due to tidal forcing, such that the linear elastic approximation holds and the resultant vertical deflection $w(x)$ is described by the Euler-Bernoulli beam bending equation, after Holdsworth (1969):

$$\frac{d^2}{dx^2}\Big[D(x)\frac{d^2w}{dx^2}\Big] = \rho_w g\big[A_0 - w(x)\big] \tag{2}$$

where A_0 is the far-field sea level, ρ_w is the mass density of seawater, g is gravitational acceleration, and D is the spatially variable flexural rigidity of the beam:

$$D(x) = \frac{Eh^3}{12(1-\nu^2)} \tag{3}$$

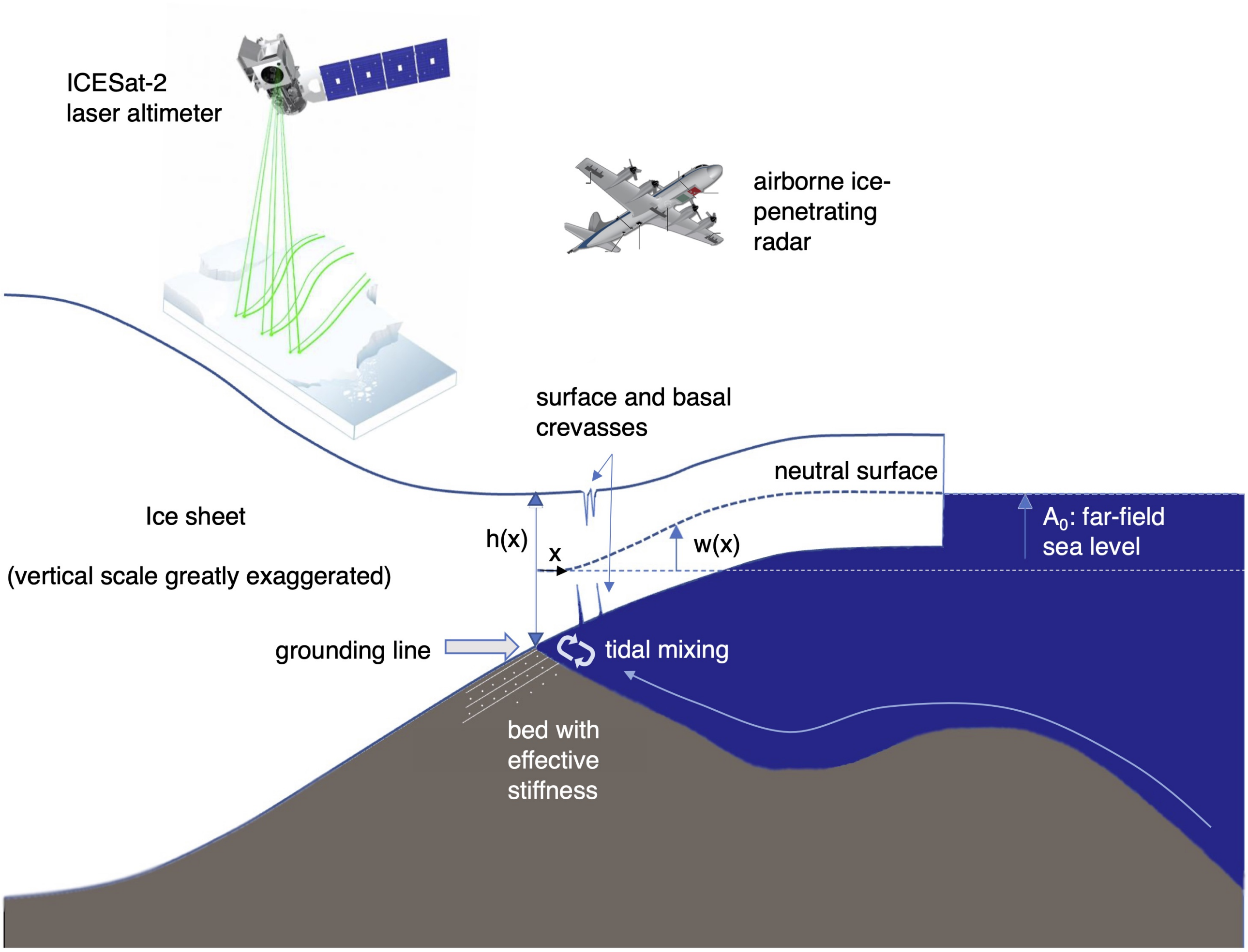

Fig. 1. We model the flexure zone as an elastic beam under tidal forcing with effective Young's modulus E*. The far-field sea level is $A_0(t)$. At $A_0 = 0$, $w(x) = 0$, and the neutral surface of our model beam rests on the x-axis. As the tide changes, the upward force on the beam is the hydrostatic pressure proportional to the difference between A_0 and $w(x)$. We can observe this flexure by differencing repeat track ice elevation measurements from ICESat-2. We allow the ice thickness in the grounding zone to vary as $h(x)$ and model the resultant combined flexure of such a beam with an effective Young's modulus E*. Surface and basal crevasses may be present. Tidal mixing takes place at the ice-ocean interface, and the grounding line may move back and forth.

where ν is the Poisson's ratio of ice, here taken to be 0.3.

To solve, we discretize Eq. 2 by central differences after Jacquot and Dewey (2001) (see supplement S1). Given full information about D, that is, h and E, the flexure of a beam under an applied forcing can be readily calculated. This is called the forward problem. The inverse problem seeks to infer properties of the beam given the flexure w. However, we will only ever be able to invert or optimize for the flexural rigidity D of the beam, that is, only one of the Young's modulus or the thickness, assuming the other is known. This problem is also ill-posed, making it sensitive to noise and resulting in solutions that may oscillate about the correct one (Lucchinetti and Stüssi, 2002).

Solving Eq. 2 requires four boundary conditions. The model results are sensitive to these boundary conditions and where they are applied. Here, we select our problem area as the flexure zone: everywhere flexure is observed to occur on tidal timescales. The landward boundary is where vertical tidal deflection vanishes. The seaward boundary is where the vertical tidal deflection reaches the constant value of A_0, the far-field sea level, which varies at each repeat track measurement. That is, $\partial w/\partial x = 0$ and $w = 0$ at $x = 0$, and $\partial w/\partial x = 0$ and $w = A_0$ at $x = L$, where L is the length of the flexure zone. This is the same set of boundary conditions used by Vaughan (1995). The length of the flexure zone and A_0 are inferred from ICESat-2 data, as described in the ICESat-2 grounding zone deflection data section.

Then, using spatially varying ice thickness from DICE (see below), we use the MATLAB patternsearch solver (The MathWorks Inc., 2022), a global optimization algorithm, to solve Eq. 2 many (e.g., hundreds or thousands) of times while varying E* to find the value of E* that minimizes the square of the misfit between the model and data. In order to manage the sensitivity of the problem to the location of the boundaries, we repeat the optimization with the landward boundary at a range of discrete points up to several kilometers upstream and downstream of its initial estimated position. This is akin to a free grounding line position, though we note that the landward extent of tidal flexure may well be upstream of the grounding line. Our method includes a grid search that sweeps across the parameter space of E* and the position of the landward boundary, seeking a minimum in the misfit space that is sensible among beams and tracks (see below boundary value grid search section). For each beam and track at each site, we infer a value for E*.

Variable ice shelf thickness data

Here we use ice thickness data from the ROSETTA-Ice airborne survey from 2015–2017 (Das and others, 2020), which uses deep ice radar (DICE) with a 188 MHz center frequency, 60 MHz bandwidth, and 1.4

m range resolution to produce a dataset of ice thickness on the Ross Ice Shelf (Figure 2). To get spatially varying ice thickness from DICE at points that are coincident with ICESat-2 ground tracks in our selected regions of interest, we use all the DICE datapoints as a scattered interpolant in order to linearly interpolate between them.

Interpreting radargrams in the grounding zone is more difficult than it is near the calving front because seawater intrusion upstream of the grounding line and grounding zone hydrodynamics can complicate delineation of the bottom surface of the ice (MacGregor and others, 2011). However, crossover analysis in Das and others (2020) was robust over the three years of data collection and were consistent to 2 m. These are among the most direct detailed measurements of ice thickness that presently exist. Continent-wide data products of ice shelf thickness typically calculate ice thickness by assuming that ice downstream of a fixed grounding line is free-floating and in hydrostatic equilibrium, then make a correction based on any existing nearby radar ice thickness measurements and interpolate (Morlighem and others, 2020). This is an excellent assumption far from the grounding line that breaks down in the grounding zone, where ice is mechanically coupled to the grounded ice sheet. In places where ice-penetrating radar data is sparse, the hydrostatic assumption systemically biases inferred ice thickness.

Boundary value grid search

The location of the inward limit of tidal flexure can migrate several kilometers on tidal timescales, as is seen in both observations and models (Freer and others, 2023; Robel and others, 2022; Stubblefield and others, 2021). This is sometimes interpreted as the grounding line position migrating on tidal timescales. While this may indeed sometimes be the case, we argue that in this application the precise location of the grounding line cannot be treated identically as the landward limit of tidal flexure, as ice is thick and some of the flexure will necessarily be transferred upstream of the grounding line. Here, we allow the landward boundary to vary for every track by performing a grid search around the initial estimated position where $\partial w/\partial x = 0$, which we first estimate as described below in the ICESat-2 grounding zone deflection data section. This implicitly allows for tidal migration of the grounding line, as well as includes any flexure of the bed that occurs below the observable surface flexure. This method is akin to a "free/stiff" configuration in the parlance of Sayag and Worster (2013), where the ice shelf rests on a stiff bed but the grounding line position is allowed to vary at different points in the tidal cycle. Note that we do not assume nor require the bed to be stiff, but rather that we use the combined flexure signal to infer the effective Young's modulus

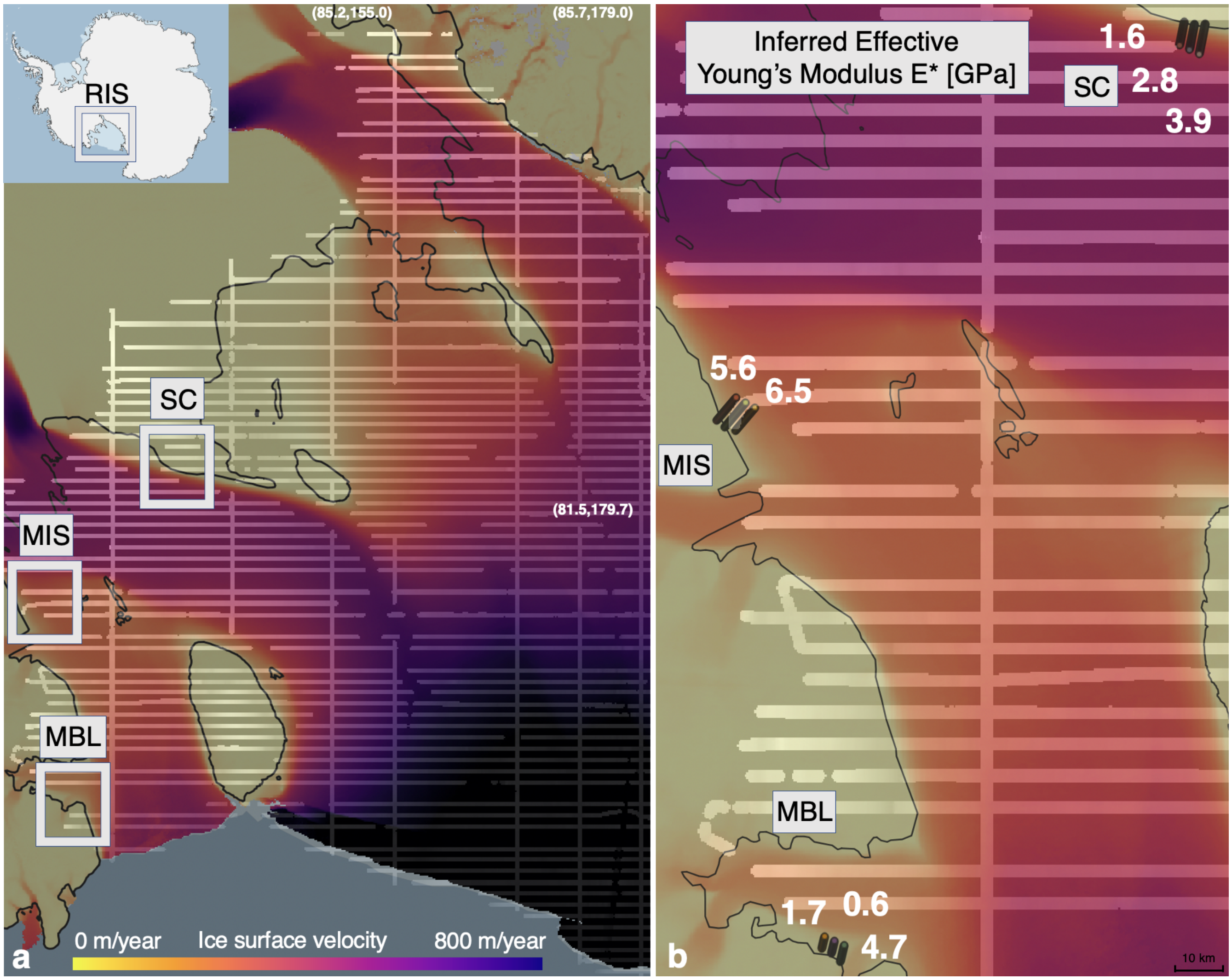

Fig. 2. The Ross Ice Shelf (RIS) and its location on the Antarctic continent (inset). The three regions studied here are highlighted: Siple Coast (SC), MacAyeal Ice Stream (MIS), and Marie Byrd Land (MBL). Study sites were chosen for their proximity to DICE measurements, distance from confining topography, and flexure data consistent with the boundary conditions we apply here. Horizontal and vertical lines show flight paths from the ROSETTA-Ice airborne ice-penetrating radar campaign (Das and others, 2020). Colors in panel (a) show ice surface velocity (Mouginot and others, 2017). Panel (b) shows the average inferred effective Young's modulus along each beam pair ground track at each site. Sections of the ICESat-2 ground tracks used for modeling are shown, dotted. Coordinates in (a) are provided at select points for spatial reference. A 10 km scalebar is shown in (b).

E*.

We repeat the optimization described above at discrete points around the initial estimated landward boundary position, first up to 1 km away in both along-track directions. We seek a well-behaved minimum in the the square of the misfit between the modeled and observed deflection. That is, a single distinct minimum within the bounds of the search, and a boundary position that makes physical sense with respect to the neighboring beams. If necessary, we extend the grid search to 2 or 4 km in either direction to meet these conditions. Figures detailing the grid searches for all data used can be found in Supplement S1.

Sometimes, there is more than one minimum in the misfit space as we vary the landward boundary position, due to the ill-posedness of the problem. In these cases, great care is taken in selecting the best result that is consistent between neighboring photon ground track pairs. Detailed information on each case is presented in Supplement S1, but generally, we also calculate the derivative of the observed flexure and use it to pick the result containing more information about the flexure.

ICESat-2 flexure zone deflection data

Tidal flexure of ice shelves can be readily observed by making repeated measurements of ice shelf surface height at different points in the tidal cycle and differencing those measurements. This has been accomplished by snowmobile (Vaughan, 1995), with ICESat (Fricker and Padman, 2006), or as here, with ICESat-2, a laser altimeter launched in 2018, which has much denser spatial resolution than ICESat, and also with radar interferometry (Freer and others, 2023; Li and others, 2022; Wild and others, 2018). We identify ICESat-2 reference ground tracks (RGTs) that cross the grounding line in three regions of the Ross Ice Shelf: Marie Byrd Land (MBL), MacAyeal Ice Stream (MIS), and the Siple Coast (SC). We used OpenAltimetry (Jodha and others, 2020) to identify ground tracks of interest that were approximately perpendicular to the grounding line in the NASA MEaSUREs Antarctic grounding line dataset (Mouginot and others, 2017) and away from confining topography that might influence the flexure.

Repeat track measurements occur at 91-day intervals. After excluding passes from 2018, when satellite pointing was not yet optimized, as well as tracks with obvious discontinuities due to cloudy conditions or other anomalous effects, 3–5 usable passes typically remain for a given photon track pair, which consists of a strong and a weak beam. We use all three photon track pairs aboard ICESat-2, which are spaced 3.3 km apart, finding a value for E∗ for each track within each pair. We report the average E∗ value across all tracks, for each photon track pair separately, in Table 1.

After processing and filtering the data as described in Supplement S1, we calculate the mean ice surface height over time using all available ground passes. We then subtract this mean height from each individual pass and apply a final smoothing step to obtain the vertical height anomaly for each track. We interpret this anomaly as the vertical tidal deflection, w, under the assumption that with enough repeat tracks, the mean height approximates the unstressed state with zero tidal amplitude.

The approximate locations of the boundaries of the grounding zone are selected visually from the ICESat-2 grounding zone deflection data. As can be seen in Figure 1, the grounding line is the point at which any landward height anomaly is flat and roughly zero. As described above, the grounding line position is allowed to vary in the inversions by up to four kilometers in either direction, which makes its visual selection appropriate as initial estimate. The precise location of the seaward boundary does not sensitively affect the result of the inversion, so long as it is far enough away to not artificially shorten the grounding zone, so it is approximated conservatively then not changed. The value of the far-field sea level, A_0, is also determined from the data as the deflection at the seaward edge of the grounding zone minus the deflection at the grounding line. When A_0 is small, little information about ice flexure can be gleaned by the inversion and these cases are left out of our analysis.

The apparent ice surface height will change as it snows. The best available data products of Antarctic precipitation in this region are available only at 25 km resolution (Wessem and others, 2018), so this could only be modeled as a constant valued offset to the observed surface. While this is visible in some of our data as an approximately constant valued offset in height anomaly landward of the grounding line, since we effectively zero the landward boundary in our model by making A_0 the difference in deflection between the seaward and landward edge of the model, we make no further correction for snow. Snowfall on the Ross Ice Shelf varies by site but is typically on the order of several centimeters to a meter of snow per year (Cohen and Dean, 2013), while the tidal amplitude is approximately one meter about once a day (Padman and others, 2018).

RESULTS

We identify three grounding zones on the Ross Ice Shelf that are far from confining topography, where DICE thickness measurements exist close to the grounding line, ICESat-2 ground tracks are roughly perpendicular to the grounding line, and where differenced ice elevation profiles show roughly zero displacement upstream of the flexure zone and roughly constant displacement downstream of the flexure zone. These are the Siple

Table 1. Inferred effective Young's modulus (E^*) in GPa at each beam and track used across three study sites on the Ross Ice Shelf. Tracks A_{1-5} correspond to dates listed in Figure 3 and are not the identical at different sites.

Site	**Beam**	A_1	A_2	A_3	A_4	A_5
SC	1	5.4	–	–	2.3	–
	2	1.4	5.4	2.5	1.6	3.0
	3	1.3	1.8	2.3	1.3	1.2
MIS	2	9.0	7.5	5.4	8.8	1.7
	3	–	4.7	–	6.4	–
MBL	1	4.3	–	–	5.0	–
	2	0.6	–	–	–	–
	3	0.8	–	–	2.6	–

Coast (SC), MacAyeal Ice Stream (MIS), and Marie Byrd Land (MBL). They are identified in Figure 2. The flexure zones are between 6 and 15 km wide between the seaward and landward boundaries as identified in the methods section. We observe that the landward boundary of the flexure zone often migrates on kilometer scales on tidal timescales.

After smoothing, filtering, and selection of approximate boundaries of the flexure zone, we run the inversion described in the Model section at each site, using each of the three beam pairs aboard ICESat-2, which are spaced 3.3 km away from each other on the ground. We find a resultant effective Young's modulus for each track, which are measured at different points in the tidal cycle. There are between one and five usable (that is, without discontinuities or other data issues, discussed further in supplement S1) tracks per beam at the sites. The average effective Young's modulus E* found across all measurements at all sites is 3.6 ± 2.5 GPa. Results for all tracks, beams, and sites are presented in Table 1.

We do not see any clear differences in effective Young's modulus in observations taken at high versus low tide. We ensure that solutions presented in Table 1 are self-consistent by verifying that the minima found in the inversion are accurately selected, that the boundary position grid search has appropriately found a minimum in misfit space, and that the flexure extent positions measured by different photon ground track pairs are plausible with respect to each other. Detailed results can be found in supplement S1.

Below, we summarize the results at each site and plot the observed and modeled flexure used to invert for the effective Young's modulus there.

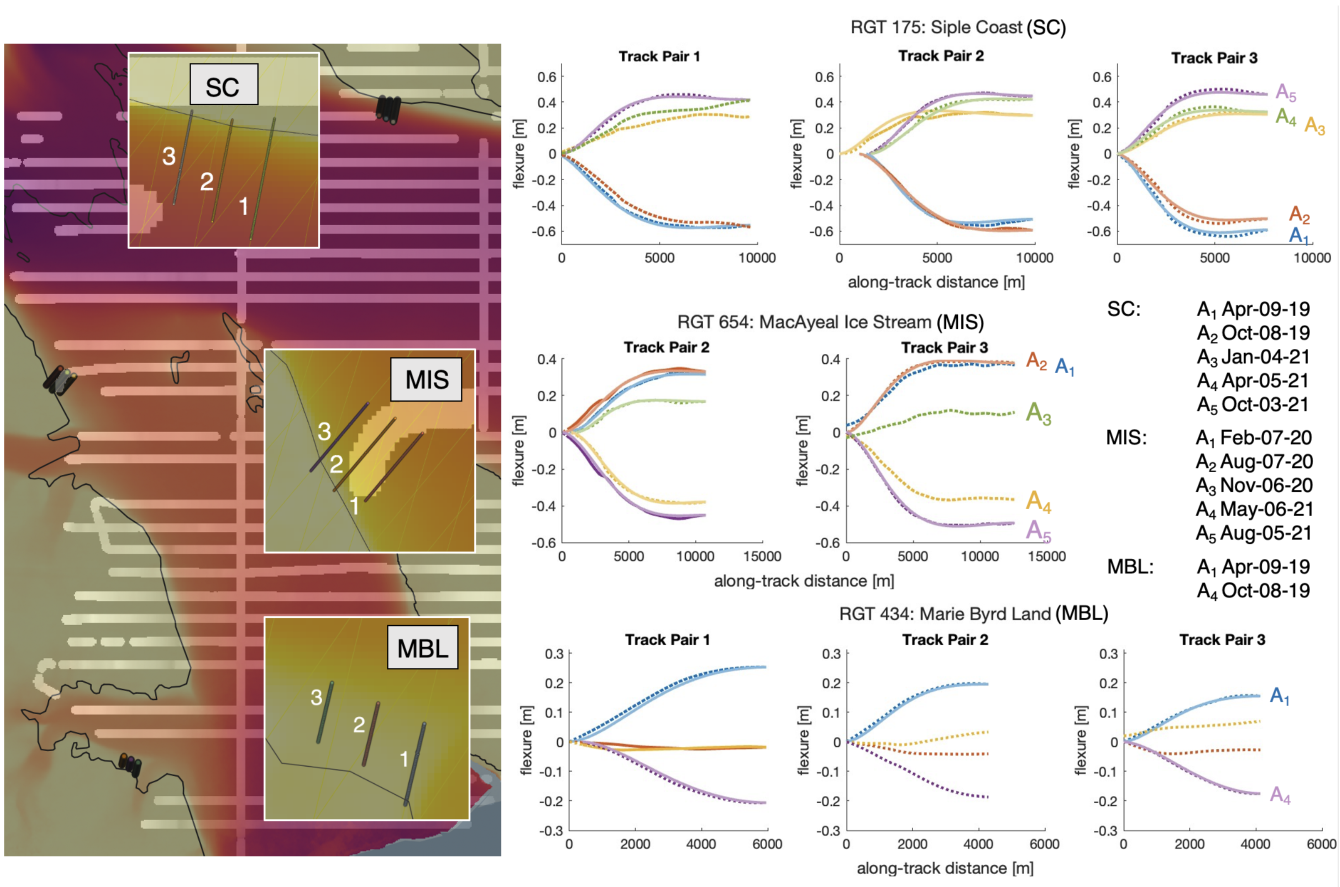

Fig. 3. Observed tidal flexure at three study sites along ICESat-2 ground tracks. (Left) The locations of the three regions: Siple Coast (SC), MacAyeal Ice Stream (MIS), and Marie Byrd Land (MBL), are shown with insets highlighting the three photon ground track pairs (1–3) used at each site. The background color map shows ice velocity (see Fig.2b) with overlying ROSETTA-Ice radar tracks. (Right) Flexure profiles for each beam, grouped by site and Reference Ground Track (RGT): RGT 175 (SC), RGT 654 (MIS), and RGT 434 (MBL). Each curve represents a measurement at a different point in the tidal cycle, labeled A_1–A_5, and corresponds to a unique date of observation (listed at right). Vertical displacement $w(x)$ is measured from repeat-track surface elevation anomalies derived from ICESat-2. Only observations with consistent flexural behavior and sufficient spatial coverage were retained for inversion. Dotted lines depict data. Solid lines depict modeled flexure.

Siple Coast

At the Siple Coast (SC) site, we observe qualitative differences in the shape of the flexure profiles across the three photon track pairs, and an average effective Young's modulus of 2.5 ± 1.4 GPa across all three. At photon track pair 1, of the five available passes, tracks 2, 3, and 5 exhibit small features within the flexure data that lead to artificially high estimates of effective Young's modulus, so we exclude them from our analysis. These features are not present at photon pairs 2 or 3, where all tracks are retained. The flexure profiles at pairs 2 and 3 yield similar effective Young's moduli. While flexure extent line positions are similar at pair 3, they migrate several hundred meters across passes at pair 2. Across all pairs and tracks, values of E* are similar at both high and low tide. We also note a slight decreasing trend in effective Young's modulus moving eastward across the site. The mean E* at photon track pairs 1, 2, and 3 is 1.6 GPa, 2.8 GPa, and 3.9 GPa, respectively.

MacAyeal Ice Stream

At MacAyeal Ice Stream (MIS), two of the three photon track pairs of RGT 654 produce usable results. Values of E* span both higher and lower than the mean at both high and low tide. Similarly, the inland flexure extent position varies by about a kilometer between tracks, without any clear correlation with tidal phase. Photon track pair 3 presents the greatest difficulty in interpreting the flexure extent grid search: the flexure extent is displaced more than 1 km from the initial estimate, and the misfit space contains multiple minima. As detailed in Supplement S1, we ultimately use tracks 2 and 4 to infer effective Young's moduli of 4.7 GPa and 6.4 GPa, respectively. In both cases, the inland extent of flexure is found to be approximately 1.5 km from the initial estimate, with no systematic difference between high and low tide. Flexure profiles at track pair 1 do not exhibit a clear transition to a flat signal beyond the tidal amplitude, so we assume our model is not applicable there and exclude them.

Marie Byrd Land

At the Marie Byrd Land (MBL) site, we observe qualitatively different flexure profiles at each track, though fewer tracks are usable in our inversion compared to the other two sites. Tracks 2 and 3 are too close to the unstressed (flat) state to be used for modeling. This site is also located closer to potential confining topography than either other site. We observe less than one kilometer of motion in the flexure extent between measurements. We use tracks 1 and 4 from photon track pairs 1 and 3, and track 1 only from pair 2. The average E* at MBL is 2.7 ± 1.8 GPa. The average inferred E* for all tracks at photon pairs 1, 2, and 3 is 4.7 GPa, 0.6 GPa, and 1.7 GPa, respectively. Potential contributors to the spread in E* values are discussed below.

DISCUSSION

We present a method for estimating effective elastic rheology near the grounding zone using tidal flexure observations from ICESat-2 and show that by varying a single effective elastic parameter in the flexure zone we can achieve excellent fits to flexure data with ice-penetrating radar ice thickness that varies in space from the ROSETTA-Ice campaign. Our results suggest that effective rheology near the grounding line may vary significantly in space.

Our model is linear elastic. Linear elasticity is an adequate approximation when the forcing timescale is short compared to the viscous relaxation timescale of ice in the grounding zone–that is, when the Deborah number $\mathrm{De} = \frac{\tau_{ve}}{\tau_{forcing}}$ is large. Taking the viscous relaxation timescale $\tau_{ve} = 2\mu/\mathrm{E}$ (Turcotte and Schubert, 2014), where μ is the dynamic viscosity, approximated as 6×10^{14} Pa s from Ranganathan and Minchew (2024), using E = 3.6 GPa, the mean value from results found here, and taking the forcing (tidal) timescale on the RIS to be approximately 12 hours (Padman and others, 2018), we find $\mathrm{De} \approx O(10)$. This indicates that while the linear elastic approximation may be valid in some grounding zones around Antarctica, care is warranted in selection of those areas, as the effective rheology of ice is increasingly observed to have strong spatial variation (Ranganathan and Minchew, 2024; Millstein and others, 2022) and there may be places where the viscous timescale is comparable to the tidal timescale.

There is no indication that the available data support differentiation between the ice and bed elasticity. Using a single effective elastic parameter is a convenient choice that allows the uncertainty associated with doing so to be quantified. In any tidal flexure model, there is a tradeoff in uncertainty in the elastic parameters of the ice or the bed or the tide selected for use in the model, which is evident in the spatial variation we find in effective Young's modulus. In addition to the known temperature and frequency dependence of E, which implicitly accounts for some anelastic effects, and the increasingly evident variation in the viscous properties of ice, there is no consensus yet about how the elastic properties of ice might differ as it exists in situ. There is basal and surface crevassing as well as microcracks, interstitial inclusions, larger grain sizes than laboratory experiments allow, air bubbles, and other effects that might be collectively parameterized as damage. Overall, our mean result of E* = 3.6 ± 2.5 GPa suggests that until we can better disentangle the intersecting processes in the grounding zone, we must either accept high uncertainty in effective rheology, or that any attempt at parameterization of the grounding zone may require a piecewise approach with different assumptions in different locations. The magnitude of this uncertainty is similar to the result of Rosier and others (2017), who find a factor of two of uncertainty in effective Young's modulus. Laboratory experiments that can more closely emulate in situ ice with inclusions or damage and at forcing frequencies close to the tidal range would be valuable in understanding the natural laboratory of the Antarctic Ice Sheet.

We did not find obvious differences in effective Young's modulus at high versus low tide at any site. This is in contrast to Sayag and Worster (2013), who find higher elastic moduli at high tide than at low tide and argue that subglacial lubrication is enhanced at high tides. We cannot rule out due to the small number of sites that tidal effects may exist, and indeed agree that subglacial hydrology may affect observable tidal flexure. However, we argue that the elastic properties of the bed and subglacial till are effectively unknown and cannot be distinguished from the flexure of the ice, and are thus incorporated into our inference of E*. First principles modeling of the subglacial environment and how it is affected by tides and how this translates to surface flexure will help step towards more accurate representation of the grounding zone in larger ice models.

Beam bending models, or plate bending models in 2D or 3D, with different boundary conditions may be able to accommodate a wider subset of ice geometries than presented here. Out of 30 candidate RGTs around the Ross Ice Shelf, only three sites were suitable enough for inclusion in the results. We select and use tracks whose flexure profiles suggest that the linear elastic approximation is a reasonable one: with smooth flexure between a flat upstream region and a flat downstream region that varies with time. We pick tracks that are roughly perpendicular to the grounding line and away from confining topography that might induce flexure in cross-track dimensions. No sites in the Transantarctic Mountains met these criteria: those tracks had different patterns of tidal deflection. Those grounding lines may also be substantially three dimensional as the ice flows off steep topography. The observable flexure on smaller scales sometimes needed to be excluded as well: beam 1 at the MIS site showed a downward flexure feature where the other two tracks remained constant seaward of the flexure zone, indicating there might be influence from other bathymetry features or in cross-track directions. Future work that seeks to parameterize grounding zone processes in larger models may need to take into account the inherent spatial variability in effective grounding zone rheology in order to accurately translate from tidal timescale processes to long-term ice sheet dynamics.

The variance in E* both among and between the sites suggest that a linear elastic parameterization works very well in some sectors and less well in others. The spread in values at the MBL site, for instance, might be noise around a mean value, but also might be related to the ill-posedness of the problem, or reflect that the nearby ice stream (see figure 3) is complicating the flexure pattern, or the subglacial system that is implicit to our parameterization. At the MIS site, values for E* cluster closely together, while at the SC site, a downward trend in E* moving eastward is reflected in our results. Finding E* in more and more continuous regions will help elucidate the true scale of spatial variance in effective Young's modulus.

The choice to parameterize the grounding zone in terms of an effective elastic rheology is both motivated by the need for an independent estimation of the ice thickness and thickness gradient there in order to calculate the basal melt rate of ice near the grounding line and also justified by the uncertainty about basal conditions in the grounding zone and of the rheology of ice. The ice flexure reveals that there is evident variability in effective rheology on sub-catchment scales; what causes this variability and how it can be parameterized in large ice models will be more and more elucidated by fundamental physics models constrained by the remote sensing data record that accumulates day by day.

CONCLUSION

We infer an effective Young's modulus of 3.6 ± 2.5 GPa from ICESat-2 data by modeling the flexure zone as an elastic beam of variable thickness. Surface flexure measurements do not readily allow us to distinguish between deformation of the bed and deformation of the ice. Therefore, the inferred elastic modulus reflects the combined flexural response of both ice and bed, along with any additive tidal or subglacial hydrological effects, as well as the in situ relationship between stress and strain in ice, which is time-dependent due to its viscoelasticity. Understanding how the effective Young's modulus varies in space at kilometer scales offers new insight into the mechanical character of the ice–bed–ocean interface, and here, is the first step in a method for making observationally constrained estimates of ice thickness and thickness gradient in the grounding zone.

Making models of Antarctica that accurately reflect its current state and recent past requires careful modeling of the grounding zone, and better parameterizations of the processes that occur there on intersecting spatial and temporal scales. Our work shows that a linear elastic model of tidal flexure could be one method for doing so, but also that it would likely need to be part of a suite of solutions encompassing viscous, viscoelastic, and viscoplastic flexure as well. The geometry of the grounding zone is complex and dynamic: different bending geometries that fit the topography on the scales over which it varies could be employed. Extending our elastic beam bending method to a viscoelastic plate bending flexure method is one clear way that more complex geometries could be represented, but the extent to which any of these potential methodologies are differentiable from one another within a small, noisy, observable signal is not yet well constrained.

The results presented here add to the constellation of estimates of the effective rheology of ice from observational and experimental methods. We are able to consider questions of variability of effective Young's modulus on small scales only because this is one of the areas where direct ice-penetrating radar measurements of ice thickness exist. In other places, ice thickness in the grounding zone is estimated by assuming ice shelves are fully free-floating and their thickness can be calculated by measuring the height of the ice above flotation. In the grounding zone, this would bias ice thickness estimates. In order to make an independent estimation of the ice thickness near the grounding line from the surface flexure, we must first make a reasonable estimation of the effective Young's modulus. More direct measurements of ice thickness in grounding zones would be a rich resource for the glaciological community as we attempt to untangle the intersecting physical processes in grounding zones, and deeply pertinent to IPCC goals toward reducing uncertainty about future sea level rise.

REFERENCES

Adusumilli S, Fricker HA, Medley B, Padman L and Siegfried MR (2020) Interannual variations in meltwater input to the southern ocean from antarctic ice shelves. *Nature Geoscience*, **13**, 616–620, ISSN 17520908 (doi: 10.1038/s41561-020-0616-z)

Alley KE, Scambos TA and Alley RB (2023) The role of channelized basal melt in ice-shelf stability: Recent progress and future priorities. *Annals of Glaciology*, **2019**, ISSN 02603055 (doi: 10.1017/aog.2023.5)

Chartrand AM and Howat IM (2023) A comparison of contemporaneous airborne altimetry and ice-thickness measurements of antarctic ice shelves. *Journal of Glaciology*, ISSN 00221430 (doi: 10.1017/jog.2023.49)

Cohen L and Dean S (2013) Snow on the ross ice shelf: comparison of reanalyses and observations from automatic weather stations. *The Cryosphere*, **7**(5), 1399–1410 (doi: 10.5194/tc-7-1399-2013)

Cuffey KM and Paterson WSB (2010) *The physics of glaciers*. Elsevier/BH,, ISBN 9780123694614

Das I, Padman L, Bell RE, Fricker HA, Tinto KJ, Hulbe CL, Siddoway CS, Dhakal T, Frearson NP, Mosbeux C, Cordero SI and Siegfried MR (2020) Multidecadal basal melt rates and structure of the ross ice shelf, antarctica, using airborne ice penetrating radar. *Journal of Geophysical Research: Earth Surface*, **125**, ISSN 21699011 (doi: 10.1029/2019JF005241)

Freer BI, Marsh OJ, Hogg AE, Fricker HA and Padman L (2023) Modes of antarctic tidal grounding line migration revealed by ice, cloud, and land elevation satellite-2 (icesat-2) laser altimetry. *Cryosphere*, **17**, 4079–4101, ISSN 19940424 (doi: 10.5194/tc-17-4079-2023)

Fricker HA and Padman L (2006) Ice shelf grounding zone structure from icesat laser altimetry. *Geophysical Research Letters*, **33**, ISSN 00948276 (doi: 10.1029/2006GL026907)

Gammon PH, Kiefte H, Clouter MJ and Denner WW (1983) Elastic constants of artificial and natural ice samples by brillouin spectroscopy. *Journal of Glaciology*, **29**, 433–460, ISSN 0022-1430 (doi: 10.3189/s0022143000030355)

Gold LW (1977) Engineering properties of fresh-water ice. *Journal of Glaciology*, **19**, 197–212, ISSN 0022-1430 (doi: 10.3189/s0022143000215608)

Gudmundsson GH, Paolo FS, Adusumilli S and Fricker HA (2019) Instantaneous antarctic ice sheet mass loss driven by thinning ice shelves. *Geophysical Research Letters*, **46**, 13903–13909, ISSN 19448007 (doi: 10.1029/2019GL085027)

Hill EA, Rosier SH, Gudmundsson GH and Collins M (2021) Quantifying the potential future contribution to global mean sea level from the filchner-ronne basin, antarctica. *Cryosphere*, **15**, 4675–4702, ISSN 19940424 (doi: 10.5194/tc-15-4675-2021)

Holdsworth G (1969) Flexure of a floating ice tongue. *Journal of Glaciology*, **8**, 385–397, ISSN 0022-1430 (doi: 10.3189/s0022143000026976)

Jacquot RG and Dewey BR (2001) Solution of static and dynamic beam bending and static buckling problems using finite differences and matlab. In *Proceedings of the 2001 American Society for Engineering Education Annual Conference & Exposition*, 6.882.1–10

Jodha S, Khalsa S, Borsa A, Nandigam V, Phan M, Lin K, Crosby C, Fricker H, Baru C and Lopez L (2020) Openaltimetry - rapid analysis and visualization of spaceborne altimeter data. *Earth Science Informatics* (doi: 10.1007/s12145-020-00520-2/Published)

Joughin I, Smith BE and Medley B (2014) Marine ice sheet collapse potentially under way for the thwaites glacier basin, west antarctica. *Science*, **344**(6185), 735–738 (doi: 10.1126/science.1249055)

Jourdain NC, Mathiot P, Merino N, Durand G, Sommer JL, Spence P, Dutrieux P and Madec G (2017) Ocean circulation and sea-ice thinning induced by melting ice shelves in the amundsen sea. *Journal of Geophysical Research: Oceans*, **122**, 2550–2573, ISSN 21699291 (doi: 10.1002/2016JC012509)

Li T, Dawson GJ, Chuter SJ and Bamber JL (2022) A high-resolution antarctic grounding zone product from icesat-2 laser altimetry. *Earth System Science Data*, **14**(2), 535–557 (doi: 10.5194/essd-14-535-2022)

Lucchinetti E and Stüssi E (2002) Measuring the flexural rigidity in non-uniform beams using an inverse problem approach. *Inverse Problems*, **18**(3), 837 (doi: 10.1088/0266-5611/18/3/320)

MacGregor JA, Anandakrishnan S, Catania GA and Winebrenner DP (2011) The grounding zone of the ross ice shelf, west antarctica, from ice-penetrating radar. *Journal of Glaciology*, **57**(205), 917–928 (doi: 10.3189/002214311798043780)

Marsh OJ, Rack W, Golledge NR, Lawson W and Floricioiu D (2014) Grounding-zone ice thickness from in-sar: Inverse modelling of tidal elastic bending. *Journal of Glaciology*, **60**, 526–536, ISSN 00221430 (doi: 10.3189/2014JoG13J033)

Millstein JD, Minchew BM and Pegler SS (2022) Ice viscosity is more sensitive to stress than commonly assumed. *Communications Earth and Environment*, **3**, ISSN 26624435 (doi: 10.1038/s43247-022-00385-x)

Morlighem M, Rignot E, Binder T, Blankenship D, Drews R, Eagles G, Eisen O, Ferraccioli F, Forsberg R, Fretwell P, Goel V, Greenbaum JS, Gudmundsson H, Guo J, Helm V, Hofstede C, Howat I, Humbert A, Jokat W, Karlsson NB, Lee WS, Matsuoka K, Millan R, Mouginot J, Paden J, Pattyn F, Roberts J, Rosier S, Ruppel A, Seroussi H, Smith EC, Steinhage D, Sun B, den Broeke MR, Ommen TD, van Wessem M and Young DA (2020) Deep glacial troughs and stabilizing ridges unveiled beneath the margins of the antarctic ice sheet. *Nature Geoscience*, **13**, 132–137, ISSN 17520908 (doi: 10.1038/s41561-019-0510-8)

Mouginot J, Scheuchl B and Rignot E (2017) Measures annual antarctic ice velocity maps, version 1 (doi: 10.5067/9T4EPQXTJYW9)

Nakayama Y, Menemenlis D, Zhang H, Schodlok M and Rignot E (2018) Origin of circumpolar deep water intruding onto the amundsen and bellingshausen sea continental shelves. *Nature Communications*, **9**, ISSN 20411723 (doi: 10.1038/s41467-018-05813-1)

Padman L, Siegfried MR and Fricker HA (2018) Ocean tide influences on the antarctic and greenland ice sheets. *Reviews of Geophysics*, **56**, 142–184, ISSN 19449208 (doi: 10.1002/2016RG000546)

Pattyn F (2017) Sea-level response to melting of antarctic ice shelves on multi-centennial timescales with the fast elementary thermomechanical ice sheet model (f.etish v1.0). *Cryosphere*, **11**, 1851–1878, ISSN 19940424 (doi: 10.5194/tc-11-1851-2017)

Pritchard HD, Ligtenberg SRM, Fricker HA, Vaughan DG, van den Broeke MR and Padman L (2012) Antarctic ice-sheet loss driven by basal melting of ice shelves. *Nature*, **484**(7395), 502–505, ISSN 1476-4687 (doi: 10.1038/nature10968)

Ranganathan M and Minchew B (2024) A modified viscous flow law for natural glacier ice: Scaling from laboratories to ice sheets. *Proceedings of the National Academy of Sciences*, **121**(23), e2309788121 (doi: 10.1073/pnas.2309788121)

Rathmann NM, Grinsted A, Mosegaard K, Lilien DA, Westhoff J, Hvidberg CS, Prior DJ, Lutz F, Thomas RE and Dahl-Jensen D (2022) Elastic wave propagation in anisotropic polycrystals: Inferring physical properties of glacier ice. *Proceedings of the Royal Society A: Mathematical, Physical and Engineering Sciences*, **478**, ISSN 14712946 (doi: 10.1098/rspa.2022.0574)

Reeh N, Christensen EL, Mayer C and Olesen OB (2003) Tidal bending of glaciers: A linear viscoelastic approach. *Annals of Glaciology*, **37**, 83–89, ISSN 02603055 (doi: 10.3189/172756403781815663)

Rignot E, Mouginot J, Morlighem M, Seroussi H and Scheuchl B (2014) Widespread, rapid grounding line retreat of pine island, thwaites, smith, and kohler glaciers, west antarctica, from 1992 to 2011. *Geophysical Research Letters*, **41**, 3502–3509, ISSN 19448007 (doi: 10.1002/2014GL060140)

Robel AA, Wilson E and Seroussi H (2022) Layered seawater intrusion and melt under grounded ice. *Cryosphere*, **16**, 451–469, ISSN 19940424 (doi: 10.5194/tc-16-451-2022)

Rosier SH, Marsh OJ, Rack W, Gudmundsson GH, Wild CT and Ryan M (2017) On the interpretation of ice-shelf flexure measurements. *Journal of Glaciology*, **63**, 783–791, ISSN 00221430 (doi: 10.1017/jog.2017.44)

Sayag R and Worster MG (2013) Elastic dynamics and tidal migration of grounding lines modify subglacial lubrication and melting. *Geophysical Research Letters*, **40**(22), 5877–5881 (doi: https://doi.org/10.1002/2013GL057942)

Scambos TA, Bell RE, Alley RB, Anandakrishnan S, Bromwich DH, Brunt K, Christianson K, Creyts T, Das SB, DeConto R, Dutrieux P, Fricker HA, Holland D, MacGregor J, Medley B, Nicolas JP, Pollard D, Siegfried MR, Smith AM, Steig EJ, Trusel LD, Vaughan DG and Yager PL (2017) How much, how fast?: A science review and outlook for research on the instability of antarctica's thwaites glacier in the 21st century (doi: 10.1016/j.gloplacha.2017.04.008)

Schulson E and Duval P (2011) *Creep and fracture of ice*. Cambridge University Press (doi: 10.3189/S0022143000206254)

Seroussi H, Nowicki S, Payne AJ, Goelzer H, Lipscomb WH, Abe-Ouchi A, Agosta C, Albrecht T, Asay-Davis X, Barthel A, Calov R, Cullather R, Dumas C, Galton-Fenzi BK, Gladstone R, Golledge NR, Gregory JM, Greve R, Hattermann T, Hoffman MJ, Humbert A, Huybrechts P, Jourdain NC, Kleiner T, Larour E, Leguy GR, Lowry DP, Little CM, Morlighem M, Pattyn F, Pelle T, Price SF, Quiquet A, Reese R, Schlegel NJ, Shepherd A, Simon

E, Smith RS, Straneo F, Sun S, Trusel LD, Breedam JV, Wal RSVD, Winkelmann R, Zhao C, Zhang T and Zwinger T (2020) Ismip6 antarctica: A multi-model ensemble of the antarctic ice sheet evolution over the 21st century (doi: 10.5194/tc-14-3033-2020)

Sinha NK (1978) Rheology of columnar-grained ice

Sinha NK (1989) Elasticity of natural types of polycrystalline ice

Smith B, Fricker HA, Gardner AS, Medley B, Nilsson J, Paolo FS, Holschuh N, Adusumilli S, Brunt K, Csatho B, Harbeck K, Markus T, Neumann T, Siegfried MR and Zwally HJ (2020) Pervasive ice sheet mass loss reflects competing ocean and atmosphere processes. *Science*, **368**(6496), 1239–1242 (doi: 10.1126/science.aaz5845)

Stubblefield AG, Spiegelman M and Creyts TT (2021) Variational formulation of marine ice-sheet and subglacial-lake grounding-line dynamics. *Journal of Fluid Mechanics*, **919**, A23 (doi: 10.1017/jfm.2021.394)

The MathWorks Inc (2022) Optimization toolbox version: 9.4 (r2022b)

Turcotte D and Schubert G (2014) *Geodynamics*. Cambridge University Press, 3 edition

Vaughan DG (1995) Tidal flexure at ice shelf margins. *Journal of Geophysical Research*, **100**, 6213–6224, ISSN 01480227 (doi: 10.1029/94JB02467)

Warburton KL, Hewitt DR and Neufeld JA (2020) Tidal grounding-line migration modulated by subglacial hydrology. *Geophysical Research Letters*, **47**, ISSN 19448007 (doi: 10.1029/2020GL089088)

Wessem JMV, Berg WJVD, Noël BP, Meijgaard EV, Amory C, Birnbaum G, Jakobs CL, Krüger K, Lenaerts JT, Lhermitte S, Ligtenberg SR, Medley B, Reijmer CH, Tricht KV, Trusel LD, Ulft LHV, Wouters B, Wuite J and Broeke MRVD (2018) Modelling the climate and surface mass balance of polar ice sheets using racmo2 - part 2: Antarctica (1979-2016). *Cryosphere*, **12**, 1479–1498, ISSN 19940424 (doi: 10.5194/tc-12-1479-2018)

Wild CT, Marsh OJ and Rack W (2018) Unraveling insar observed antarctic ice-shelf flexure using 2-d elastic and viscoelastic modeling. *Frontiers in Earth Science*, **6**, ISSN 22966463 (doi: 10.3389/feart.2018.00028)

Wåhlin A, Alley KE, Begeman C, Øyvind Hegrenaes, Yuan X, Graham AGC, Hogan K, Davis PED, Dotto TS, Eayrs C, Hall RA, Holland DM, Kim TW, Larter RD, Ling L, Muto A, Pettit EC, Schmidt BE, Snow T, Stedt F, Washam PM, Wahlgren S, Wild C, Wellner J, Zheng Y and Heywood KJ (2024) Swirls and scoops: Ice base melt revealed by multibeam imagery of an antarctic ice shelf. *Sci. Adv*, **10**, 31